JOURNAL OF GUIDANCE, CONTROL, AND DYNAMICS
Vol. 29, No. 5, September–October 2006

Periodic Orbits with Low-Thrust Propulsion in the Restricted Three-Body Problem

Mutsuko Morimoto*
Graduate University for Advanced Studies, Sagamihara 229-8510, Japan
and
Hiroshi Yamakawa† and Kuninori Uesugi‡
Japan Aerospace Exploration Agency, Sagamihara 229-8510, Japan

DOI: 10.2514/1.19079

Periodic orbits around nonequilibrium points are generated systematically by using continuous low-thrust propulsion in the restricted three-body problem, with a mass ratio varying from 0 to 1/2. A continuous constant acceleration is applied to cancel the gravitational forces of two primary bodies and the centrifugal force at a nonequilibrium point, which is changed into an artificial equilibrium point. The equations of motion are linearized to analytically generate periodic orbits with constant acceleration. Then, periodic orbits around artificial equilibrium points which exist on the line connecting two primary bodies are investigated. The frequencies of these periodic motions are expressed by a parameter that is a function of the mass ratio and the position of the orbits around artificial equilibrium points. By choosing the frequencies of motions that are small-integer resonant, we have found the existence of points at which in-plane and out-of-plane motions are synchronized.

Nomenclature

A, B, C	=	nondimensional amplitudes of oscillation
$\mathbf{a}$	=	nondimensional acceleration vector in rotating frame
C_j	=	constants of integration
i	=	$\sqrt{-1}$
k	=	$s^2 (k = \lambda + i\theta)$
n	=	the number of characteristic solutions
P	=	parameter as a function of mass ratio and position of artificial equilibrium point
Q, Q_1, Q_2	=	matrices for characteristic equation
$\mathbf{r}$	=	nondimensional position vector from origin to spacecraft
r_1, r_2	=	nondimensional distance from origin to two primary bodies
s	=	characteristic solutions ($s = \sigma + i\varphi$)
U	=	$U^* + \Phi$
U^*	=	nondimensional gravitational potential
α, β, γ	=	values of solution k
μ	=	mass ratio
μ_1, μ_2	=	nondimensional gravitational constant of two primary bodies
$\boldsymbol{\delta}(\delta_x, \delta_y, \delta_z)$	=	nondimensional vector from artificial equilibrium point to spacecraft
Φ	=	nondimensional centrifugal potential
ϕ	=	initial phase angle, rad
$\boldsymbol{\omega}$	=	nondimensional angular velocity vector of rotating frame
ω	=	nondimensional circular frequency

Subscripts

x	=	with respect to the x axis
y	=	with respect to the y axis
z	=	with respect to the z axis
0	=	with respect to the artificial equilibrium point

I. Introduction

THIS paper describes an investigation of periodic orbits obtained through linearization about artificial equilibrium points in the restricted three-body problem. In this problem, there are five equilibrium points, known as "Lagrange points," each of which is in equilibrium between the gravitational forces of the two primary bodies and the centrifugal force in the rotating frame. When forces produced by low-thrust propulsion are considered, artificial equilibrium points that differ from the Lagrange points can be obtained. This paper studies periodic motions in the vicinity of such equilibrium points.

Since the 1950s, numerous studies regarding equilibrium points in the restricted three-body problem and periodic orbits around these points have been reported. Broucke [1] studied ballistic periodic orbits systematically in the elliptic restricted three-body problem for the entire ranges of eccentricity and mass ratio, and seven general classes of periodic orbits were identified. Farquhar [2] generated ballistic periodic (station keeping) orbits in the vicinity of the unstable colinear libration points, L_1 and L_2, by linearizing the equation of motion. As the frequency differs between the in-plane and out-of-plane oscillations, the projections are Lissajous curves. Therefore, by considering nonlinear effects, quasiperiodic orbits known as halo orbits were obtained [3]. However, these orbits have a constraint on their amplitude. Jorba [4] focused on the dynamics near the colinear equilibrium points and obtained an accurate description of the dynamics by a combination of the reduction to the center manifold and the Lindstedt–Poincaré method. Gómez [5] also analyzed an extended neighborhood of the colinear equilibrium points in which all the relevant information of the neutrally stable behavior of the dynamics was given. Dusek [6] discussed possible regions of libration points as a function of low-thrust forces in two-dimensional space and showed that artificial equilibrium (libration) points can be generated by constant radial low-thrust forces. He also reported that, by varying the forces as a function of the distance from the center, the motion around a point becomes a largely stable orbit.

Received 24 July 2005; revision received 30 December 2005; accepted for publication 23 January 2006.

*Graduate Student, Department of Space and Astronautical Science, 3-1-1, Yoshinodai, Sagamihara 229-8510, Japan.

†Associate Professor, Institute of Space and Astronautical Science, Department of Space Systems and Astronautics. Member AIAA.

‡Professor, Institute of Space and Astronautical Science, Department of Space Systems and Astronautics.

Simmons [7] studied equilibrium points in the restricted three-body problem modified by radiation pressure from two finite masses, for the entire mass ratio range. He reported nine equilibrium points exist (five points in the orbital plane and four points out of the orbital plane,) when the radiation pressure of the smaller mass is very high. McInnes [8] investigated artificial equilibrium points (stationary solutions) in three-dimensional space for the Earth–sun and Earth–moon systems using solar sails with the limitation that the acceleration must be in the direction away from the sun. Scheeres [9] analyzed a control law which stabilizes unstable periodic halo orbits about an Earth–sun libration point with continuous acceleration assuming Hill's problem and discussed applications to formation flight. Broschart [10] investigated hovering with constant thrust about a small body.

In summary, these previous studies have investigated periodic orbits for two primary bodies with a certain mass ratio, those around Lagrange points, and those with radial low-thrust accelerations. However, there have been no past analytical studies regarding periodic orbits with low-thrust acceleration by any types of propulsion systems and those for the whole mass ratio range.

In this study, using continuous low-thrust accelerations, we systematically generate three-dimensional periodic orbits in the circular restricted three-body problem for the entire mass ratio range of the two primary bodies. The results can be applied to any combinations of two primary bodies in the solar system such as the Earth–moon, the Earth–sun, sun–minor body, Pluto–Charon, binary asteroids, and Jupiter–Europa systems. The equations of motion are linearized around the artificial equilibrium points and solved analytically. The periodic orbits around a point on the line connecting two primary bodies are studied. In particular, the in-plane and out-of-plane resonant motions on this line are investigated in detail. As a result, we have found that resonant periodic orbits with a simple integer ratio can be realized by defining an artificial equilibrium point around which a low-thrust spacecraft orbits and its acceleration, under the above conditions.

II. Equations of Motion

A. Equations of Motion and Acceleration for Artificial Equilibrium Points

The problem of the motion of a negligible mass (i.e., spacecraft) moving under the gravitational influence of two primary masses is called the restricted three-body problem. The two masses are assumed to have circular orbits about their common center of mass and to gravitationally attract the spacecraft, although the spacecraft does not affect the two masses [11,12].

A rotating frame (x, y, z), in which the two primary masses are fixed on the x axis (Fig. 1), is used in the present study. The y axis is in the coplane of two primary bodies and the z axis is defined so as to constitute a right-handed system. The masses of the primary bodies are made nondimensional as

$$\mu_1 = 1 - \mu \tag{1}$$

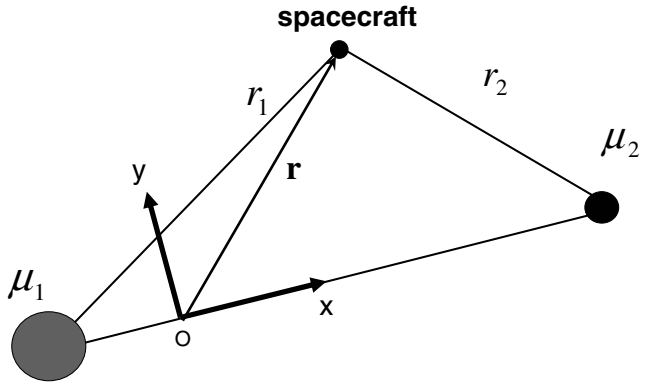

Fig. 1 Rotating frame and relationship between two primary bodies and spacecraft.

$$\mu_2 = \mu \tag{2}$$

where $0 < \mu < 1/2$.

The distance between the two primaries is taken to be unity, and the orbital period of the primary bodies is set to 2π. The distances between the spacecraft and two primary bodies are expressed, respectively, as

$$r_1^2 = (x + \mu_2)^2 + y^2 + z^2, \qquad r_2^2 = (x - \mu_1)^2 + y^2 + z^2 \tag{3}$$

The equation of motion of the spacecraft is then expressed as

$$\frac{\mathrm{d}^2\mathbf{r}}{\mathrm{d}t^2} + 2\boldsymbol{\omega} \times \frac{\mathrm{d}\mathbf{r}}{\mathrm{d}t} + \boldsymbol{\omega} \times (\boldsymbol{\omega} \times \mathbf{r}) = \mathbf{a} - \nabla U^*(\mathbf{r}) \tag{4}$$

where $\mathbf{a}$ is the control acceleration and $U^*(\mathbf{r})$ is given by

$$U^*(\mathbf{r}) = -\left(\frac{\mu_1}{r_1} + \frac{\mu_2}{r_2}\right) \tag{5}$$

The centrifugal term in Eq. (4) is written as

$$\nabla\Phi = \boldsymbol{\omega} \times (\boldsymbol{\omega} \times \mathbf{r}), \qquad \Phi(\mathbf{r}) = -\tfrac{1}{2}|\boldsymbol{\omega} \times \mathbf{r}|^2 \tag{6}$$

The new scalar function is then defined as

$$U(\mathbf{r}) = U^*(\mathbf{r}) + \Phi(\mathbf{r}) \tag{7}$$

Therefore, Eq. (4) can be rewritten as

$$\frac{\mathrm{d}^2\mathbf{r}}{\mathrm{d}t^2} + 2\boldsymbol{\omega} \times \frac{\mathrm{d}\mathbf{r}}{\mathrm{d}t} + \nabla U(\mathbf{r}) - \mathbf{a} = 0 \tag{8}$$

An artificial equilibrium point with low thrust is obtained by determining $\mathbf{a}_0$ satisfying the following equation:

$$\nabla U(\mathbf{r}_0) - \mathbf{a}_0 = \mathbf{0} \tag{9}$$

Therefore, a nonequilibrium point $\mathbf{r}_0$ is changed into an artificial equilibrium point with low-thrust acceleration, $\mathbf{a}(\mathbf{r}_0) = \nabla U(\mathbf{r}_0)$ [8].

Note that Lagrange points are obtained by taking $\mathbf{a}_0 = \mathbf{0}$ [i.e., $\nabla U(\mathbf{r}) = \mathbf{0}$].

B. Linearization

To keep the spacecraft at a nonequilibrium point, a continuous acceleration is given to the spacecraft. In this section the equations of motion in the vicinity of such a nonequilibrium point are derived. The spacecraft orbits around the artificial equilibrium points $(\mathbf{r}_0)$ with continuous acceleration which is assumed to be constant during an orbit. The equations are linearized about an artificial equilibrium point keeping the acceleration constant.

Using $\mathbf{r} = \mathbf{r}_0 + \boldsymbol{\delta}[\boldsymbol{\delta} = (\delta_x, \delta_y, \delta_z)]$, the linearized equations of motion are obtained as [8]

$$\frac{\mathrm{d}^2\boldsymbol{\delta}}{\mathrm{d}t^2} + 2\boldsymbol{\omega} \times \frac{\mathrm{d}\boldsymbol{\delta}}{\mathrm{d}t} + \nabla U(\mathbf{r}_0) + \left[\frac{\partial}{\partial \mathbf{r}} \nabla U(\mathbf{r})\right]_{r_0} \boldsymbol{\delta} - \mathbf{a}(\mathbf{r}_0) - \left[\frac{\partial}{\partial \mathbf{r}} \mathbf{a}(\mathbf{r})\right]_{r_0} \boldsymbol{\delta} = 0 \tag{10}$$

Assuming that the continuous acceleration is constant in the rotating frame we have

$$\left[\frac{\partial}{\partial \mathbf{r}} \mathbf{a}(\mathbf{r})\right]_{r_0} = 0 \tag{11}$$

By Eqs. (9) and (11), Eq. (10) is rewritten as

$$\frac{\mathrm{d}^2\boldsymbol{\delta}}{\mathrm{d}t^2} + 2\boldsymbol{\omega} \times \frac{\mathrm{d}\boldsymbol{\delta}}{\mathrm{d}t} + \left[\frac{\partial}{\partial \mathbf{r}} \nabla U(\mathbf{r})\right]_{r_0} \boldsymbol{\delta} = 0 \tag{12}$$

These are the equations of motion around an artificial equilibrium point $(\mathbf{r}_0)$ with a constant acceleration $\mathbf{a}(\mathbf{r}_0)$ in the rotating frame.

The third term of Eq. (12) is expressed in matrix form as

$$\left[\frac{\partial}{\partial \mathbf{r}}\nabla U(\mathbf{r})\right]_{r_0} = \begin{bmatrix} U_{xx} & U_{xy} & U_{xz} \\ U_{yx} & U_{yy} & U_{yz} \\ U_{zx} & U_{zy} & U_{zz} \end{bmatrix} \tag{13}$$

The elements of this matrix are shown to be

$$\begin{cases} U_{xx} = -1 + P_3 - 3(x+\mu_2)^2 P_1 + P_4 - 3(x-\mu_1)^2 P_2 \\ U_{yy} = -1 + P_3 - 3y^2 P_1 + P_4 - 3y^2 P_2 \\ U_{zz} = P_3 - 3z^2 P_1 + P_4 - 3z^2 P_2 \\ U_{xy} = U_{yx} = -3y\{(x+\mu_2)P_1 + (x-\mu_1)P_2\} \\ U_{xz} = U_{zx} = -3z\{(x+\mu_2)P_1 + (x-\mu_1)P_2\} \\ U_{yz} = U_{zy} = -3yz(P_1 + P_2) \end{cases} \tag{14}$$

where

$$\begin{cases} P_1 = \mu_1 r_1^{-5} \\ P_2 = \mu_2 r_2^{-5} \\ P_3 = \mu_1 r_1^{-3} \\ P_4 = \mu_2 r_2^{-3} \end{cases} \tag{15}$$

Here, we have

$$2\boldsymbol{\omega} \times \boldsymbol{\delta} = \begin{bmatrix} 0 \\ 0 \\ 2 \end{bmatrix} \times \begin{bmatrix} \delta_x \\ \delta_y \\ \delta_z \end{bmatrix} \tag{16}$$

Therefore, Eq. (12) is also written as

$$\frac{\mathrm{d}^2}{\mathrm{d}t^2}\begin{bmatrix} \delta_x \\ \delta_y \\ \delta_z \end{bmatrix} + \frac{\mathrm{d}}{\mathrm{d}t}\begin{bmatrix} -2\delta_y \\ 2\delta_x \\ 0 \end{bmatrix} + \begin{bmatrix} U_{xx} & U_{xy} & U_{xz} \\ U_{yx} & U_{yy} & U_{yz} \\ U_{zx} & U_{zy} & U_{zz} \end{bmatrix}\begin{bmatrix} \delta_x \\ \delta_y \\ \delta_z \end{bmatrix} = \mathbf{0} \tag{17}$$

C. Solution of the Linearized Equations of Motion

In this section, the linearized equations of motion are solved. Suppose that $\delta_x = e^{st}(s = \sigma + i\varphi)$ in Eq. (17). Then, we have

$$\begin{cases} \dot{\delta}_x = s e^{st} = s\delta_x \\ \ddot{\delta}_x = s^2 e^{st} = s^2 \delta_x \end{cases} \tag{18}$$

By substituting these and similar equations into Eq. (17), we have

$$\begin{bmatrix} s^2 + U_{xx} & -2s + U_{xy} & U_{xz} \\ 2s + U_{yx} & s^2 + U_{yy} & U_{yz} \\ U_{zx} & U_{zy} & s^2 + U_{zz} \end{bmatrix}\begin{bmatrix} \delta_x \\ \delta_y \\ \delta_z \end{bmatrix} = \mathbf{0} \tag{19}$$

Let the first matrix on the left-hand side of Eq. (19) be defined as

$$\mathbf{Q} = \begin{bmatrix} s^2 + U_{xx} & -2s + U_{xy} & U_{xz} \\ 2s + U_{yx} & s^2 + U_{yy} & U_{yz} \\ U_{zx} & U_{zy} & s^2 + U_{zz} \end{bmatrix} \tag{20}$$

Thus, the characteristic equation is written as $\det \mathbf{Q}$, where

$$\begin{aligned} \det \mathbf{Q} = {} & s^6 + (U_{xx} + U_{yy} + U_{zz} + 4)s^4 + (U_{xx}U_{yy} + U_{xx}U_{zz} \\ & + U_{yy}U_{zz} - U_{xy}^2 - U_{xz}^2 - U_{yz}^2 + 4U_{zz})s^2 + U_{xx}U_{yy}U_{zz} \\ & + 2U_{xy}U_{xz}U_{yz} - U_{yz}^2 U_{xx} - U_{xz}^2 U_{yy} - U_{xy}^2 U_{zz} \end{aligned} \tag{21}$$

From Eqs. (14) and (15), the second term of Eq. (21) is

$$U_{xx} + U_{yy} + U_{zz} + 4 = 2 \tag{22}$$

then

$$\begin{aligned} \det \mathbf{Q} = {} & s^6 + 2s^4 + (U_{xx}U_{yy} + U_{xx}U_{zz} + U_{yy}U_{zz} - U_{xy}^2 - U_{xz}^2 \\ & - U_{yz}^2 + 4U_{zz})s^2 + U_{xx}U_{yy}U_{zz} + 2U_{xy}U_{xz}U_{yz} - U_{yz}^2 U_{xx} \\ & - U_{xz}^2 U_{yy} - U_{xy}^2 U_{zz} \end{aligned} \tag{23}$$

When we set $k = s^2$, $\det \mathbf{Q}$ is rewritten as

$$\begin{aligned} \det \mathbf{Q} = {} & k^3 + 2k^2 + (U_{xx}U_{yy} + U_{xx}U_{zz} + U_{yy}U_{zz} - U_{xy}^2 - U_{xz}^2 \\ & - U_{yz}^2 + 4U_{zz})k + U_{xx}U_{yy}U_{zz} + 2U_{xy}U_{xz}U_{yz} - U_{yz}^2 U_{xx} \\ & - U_{xz}^2 U_{yy} - U_{xy}^2 U_{zz} \end{aligned} \tag{24}$$

To solve Eq. (17), the characteristic solutions s must satisfy

$$\det \mathbf{Q} = \mathbf{0} \tag{25}$$

Equation (24) is a cubic equation of k, so that the solutions k of Eq. (25) can be obtained analytically and therefore, characteristic solutions for s are also obtained analytically by $s = \pm\sqrt{k}$.

Solutions of Eq. (25) can be generally expressed in the form $k = \lambda + i\theta$. Thus, the characteristic solutions are also written as $s = \sigma + i\varphi$, since $k = s^2$.

In general, when characteristic solutions $s_j = \sigma \pm i\varphi (j = 1, \ldots, n)$ are obtained, the motion δ is expressed as

$$\begin{aligned} \boldsymbol{\delta} &= \sum_{j=1}^{n} \mathbf{C}_j e^{s_i t} = \sum_{j=1}^{n} \mathbf{C}_j e^{(\sigma \pm i\varphi)t} = \sum_{j=1}^{n} \mathbf{C}_j e^{\sigma t} e^{\pm i\varphi t} \\ &= \sum_{j=1}^{n} \mathbf{C}_j e^{\sigma t}(\cos\varphi t \pm i \sin\varphi t) \end{aligned} \tag{26}$$

where n is the number of characteristic solutions and $\mathbf{C}_j$ are constants of integration.

When the characteristic solutions s contain a real number (i.e., $s = \sigma + i\varphi$ or $s = \sigma$), the motion of the spacecraft experiences either damping or divergence. When the characteristic solutions s are purely imaginary (i.e., $s = i\varphi$), the motion oscillates. Therefore, if at least one purely imaginary solution is contained among the characteristic solutions, oscillatory motions are obtained by determining the initial value to set the divergence term to zero.

In general, solutions of the cubic equation are either 1) all real numbers or 2) one solution is a real number and the other solutions are imaginary numbers. From $k = s^2$, s is decided to be a real number or an imaginary number based on the sign of k. Therefore, to obtain a purely imaginary characteristic solution, k must have at least one negative real solution for the motion to be oscillating.

III. Oscillatory Motion

Next, we consider linearized orbits about $\mathbf{r}_0 = (X_0, Y_0, Z_0)$ $(X_0 \neq 0, Y_0 = 0, Z_0 = 0)$. Substituting $(X_0, 0, 0)$ into Eq. (3) results in

$$r_1^2 = (X_0 + \mu_2)^2, \qquad r_2^2 = (X_0 - \mu_1)^2 \tag{27}$$

Using the relation shown in Eq. (15),

$$\begin{cases} P_1 = (1-\mu)|X_0 + \mu|^{-5} \\ P_2 = \mu|X_0 + \mu - 1|^{-5} \\ P_3 = (1-\mu)|X_0 + \mu|^{-3} \\ P_4 = \mu|X_0 + \mu - 1|^{-3} \end{cases} \tag{28}$$

and we obtain

$$\begin{cases} U_{xx} = -1 - 2(1-\mu)|X_0+\mu|^{-3} - 2\mu|X_0+\mu-1|^{-3} \\ U_{yy} = -1 + \mu|X_0+\mu-1|^{-3} + (1-\mu)|X_0+\mu|^{-3} \\ U_{zz} = \mu|X_0+\mu-1|^{-3} + (1-\mu)|X_0+\mu|^{-3} \\ U_{xy} = U_{yx} = 0 \\ U_{xz} = U_{zx} = 0 \\ U_{yz} = U_{zy} = 0 \end{cases} \tag{29}$$

Here a new parameter $P(X_0, \mu)$ is introduced,

$$P(X_0, \mu) = \mu|X_0+\mu-1|^{-3} + (1-\mu)|X_0+\mu|^{-3} \tag{30}$$

Given that $\mu > 0$ and $1 - \mu > 0$, we have

$$P(X_0, \mu) > 0 \tag{31}$$

Finally, Eq. (17) is rewritten as

$$\begin{cases} \ddot{\delta}_x - 2\dot{\delta}_y - (2P+1)\delta_x = 0 \\ \ddot{\delta}_y + 2\dot{\delta}_x + (P-1)\delta_y = 0 \\ \ddot{\delta}_z + P\delta_z = 0 \end{cases} \tag{32}$$

and Eq. (19) becomes

$$\begin{bmatrix} Q_1 & & 0 \\ & & 0 \\ 0 & 0 & Q_2 \end{bmatrix} \begin{bmatrix} \delta_x \\ \delta_y \\ \delta_z \end{bmatrix} = \mathbf{0} \tag{33}$$

where

$$Q_1 = \begin{bmatrix} s^2 - 2P - 1 & -2s \\ 2s & s^2 + P - 1 \end{bmatrix}, \qquad Q_2 = \lfloor s^2 + P \rfloor$$

Here, the equation of motion for δ_z is independent of those for δ_x and δ_y.

A. In-Plane Motion

To obtain the solutions δ_x and δ_y, the characteristic equation of Q_1 is written as

$$\det Q_1 = (s^2 - 2P - 1)(s^2 + P - 1) + 4s^2 = s^4 - (P-2)s^2 - (2P+1)(P-1) \tag{34}$$

The characteristic solutions must satisfy

$$\det Q_1 = 0 \tag{35}$$

When we set $k = s^2$,

$$k^2 - (P-2)k - (2P+1)(P-1) = 0 \tag{36}$$

is obtained. Therefore, solving for k, we have

$$k = s^2 = \frac{P(X_0,\mu) - 2 \pm \sqrt{9P(X_0,\mu)^2 - 8P(X_0,\mu)}}{2} \tag{37}$$

When k is real and negative, the motions of δ_x and δ_y may become oscillatory.

A precondition for this to occur is that

$$9P(X_0,\mu)^2 - 8P(X_0,\mu) \geq 0 \tag{38}$$

which is satisfied if

$$P(X_0,\mu) \leq 0 \quad \text{or} \quad P(X_0,\mu) \geq \tfrac{8}{9} \tag{39}$$

Here, the real solutions ($k = \alpha, \beta$) are defined as

$$\alpha = \frac{P(X_0,\mu) - 2 + \sqrt{9P(X_0,\mu)^2 - 8P(X_0,\mu)}}{2} \tag{40}$$

and

$$\beta = \frac{P(X_0,\mu) - 2 - \sqrt{9P(X_0,\mu)^2 - 8P(X_0,\mu)}}{2} \tag{41}$$

To obtain oscillatory motions of δ_x and δ_y, the condition $\alpha, \beta < 0$, must also be satisfied.

For $\alpha < 0$, the condition of $P(X_0, \mu)$ is

$$-\tfrac{1}{2} < P(X_0,\mu) < 1 \tag{42}$$

and for $\beta < 0$

$$\text{for all volumes of } P(X_0,\mu) \tag{43}$$

B. Out-of-Plane Motion

Next, the out-of-plane motion δ_z is obtained by solving

$$Q_2 = s^2 + P = 0 \tag{44}$$

Then, by $k = s^2$ Eq. (44) is rewritten as

$$k + P = 0 \tag{45}$$

When the solution of Eq. (45) is expressed in terms of γ, $\gamma = -P$. Therefore, γ is a real number because $P(X, \mu)$ is real. In order that the motions of δ_z oscillate, $\gamma < 0$ must be satisfied, that is

$$P > 0 \tag{46}$$

C. Oscillatory Motion Condition

Figure 2 shows the characteristic roots with respect to $P(X_0, \mu)$. From Eq. (31), $P(X_0, \mu)$ must be greater than 0. From this figure, the condition is divided into three regions according to $P(X_0, \mu)$. I: [$P(X, \mu) \geq 1$, s^2 is a real number, $\alpha > 0$, $\beta < 0$, $\gamma < 0$]; II: [$8/9 \leq P(X, \mu) < 1$, s^2 is a real number $\alpha < 0, \beta < 0, \gamma < 0$]; and III: [$0 < P(X, \mu) \leq 8/9$, s^2 is an imaginary number, $\alpha < 0$, $\beta < 0$, $\gamma < 0$]. The shaded area in the first line denotes that $P(X_0, \mu)$ must not exist in this range due to Eq. (31). Conditions 1–4 are the oscillation or divergence conditions that occur in Eqs. (39), (42), (43), and (46). Note that region III corresponds to a stable region.

1. Region I

The characteristic solutions for δ_x and δ_y contain both real numbers ($s = \pm\sqrt{\alpha}$) and imaginary numbers ($s = \pm\sqrt{-\beta}i$), and those for δ_z are imaginary numbers [$s = \pm\sqrt{P(X_0,\mu)}i$]. Therefore, the solution $\boldsymbol{\delta}$ is obtained as follows:

$$\begin{cases} \delta_x = A_1 e^{\sqrt{\alpha}t} + A_2 e^{-\sqrt{\alpha}t} + A_3 \cos\sqrt{-\beta}t + A_4 \sin\sqrt{-\beta}t \\ \delta_y = A_5 e^{\sqrt{\alpha}t} + A_6 e^{-\sqrt{\alpha}t} + A_7 \cos\sqrt{-\beta}t + A_8 \sin\sqrt{-\beta}t \\ \delta_z = A_9 \cos\sqrt{P(X_0,\mu)}t + A_{10} \sin\sqrt{P(X_0,\mu)}t \end{cases} \tag{47}$$

where $A_i (i = 1, \ldots, 10)$ are constants of integration.

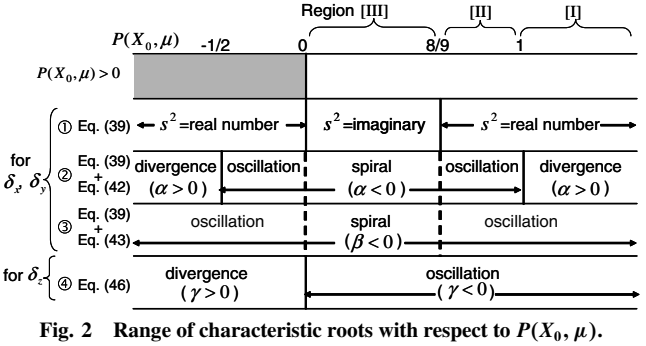

Fig. 2 Range of characteristic roots with respect to $P(X_0, \mu)$.

When we set $\omega_\beta(X_0,\mu)=\sqrt{-\beta}$ and $\omega_z(X_0,\mu)=\sqrt{P(X_0,\mu)}$ and choose only the oscillation term from these equations, the motions are rewritten as

$$\begin{cases}\delta_x = k_\beta A\cos(\omega_\beta t+\phi_{xy})\\ \delta_y = A\sin(\omega_\beta t+\phi_{xy})\\ \delta_z = A_z\cos(\omega_z t+\phi_z)\end{cases} \tag{48}$$

where

$$k_\beta=\frac{2\omega_\beta(X_0,\mu)}{\omega_\beta(X_0,\mu)^2+2P(X_0,\mu)+1} \tag{49}$$

2. Region II

The characteristic solutions for δ_x and δ_y are all imaginary numbers ($s=\pm\sqrt{-\alpha}i,\pm\sqrt{-\beta}i$), and those for δ_z are imaginary numbers [$s=\pm\sqrt{P(X_0,\mu)}i$]. Therefore, the motions of $\boldsymbol{\delta}$ are obtained as follows:

$$\begin{cases}\delta_x = B_1\cos\sqrt{-\alpha}t+B_2\sin\sqrt{-\alpha}t+B_3\cos\sqrt{-\beta}t+B_4\sin\sqrt{-\beta}t\\ \delta_y = B_5\cos\sqrt{-\alpha}t+B_6\sin\sqrt{-\alpha}t+B_7\cos\sqrt{-\beta}t+B_8\sin\sqrt{-\beta}t\\ \delta_z = B_9\cos\sqrt{P(X_0,\mu)}t+B_{10}\sin\sqrt{P(X_0,\mu)}t\end{cases} \tag{50}$$

where $B_i(i=1,\ldots,10)$ are constants of integration.

When we set $\omega_\beta(X_0,\mu)=\sqrt{-\beta}$, $\omega_\beta(X_0,\mu)=\sqrt{-\beta}$, and $\omega_z(X_0,\mu)=\sqrt{P(X_0,\mu)}$, and choose only the oscillation term from these equations, the motions are rewritten as

$$\begin{cases}\delta_x = k_\alpha B\cos(\omega_\alpha t+\phi_{xy})\\ \delta_y = B\sin(\omega_\alpha t+\phi_{xy})\\ \delta_z = B_z\cos(\omega_z t+\phi_z)\end{cases} \tag{51}$$

or

$$\begin{cases}\delta_x = k_\beta B\cos(\omega_\beta t+\phi_{xy})\\ \delta_y = B\sin(\omega_\beta t+\phi_{xy})\\ \delta_z = B_z\cos(\omega_z t+\phi_z)\end{cases} \tag{52}$$

where

$$\begin{aligned}k_\alpha&=\frac{2\omega_\alpha(X_0,\mu)}{\omega_\alpha(X_0,\mu)^2+2P(X_0,\mu)+1},\\ k_\beta&=\frac{2\omega_\beta(X_0,\mu)}{\omega_\beta(X_0,\mu)^2+2P(X_0,\mu)+1}\end{aligned} \tag{53}$$

and δ_x and δ_y each have two frequencies, either of which may be chosen.

3. Region III

The characteristic solutions for δ_x and δ_y are all real numbers ($s=\pm\sqrt{\alpha},\pm\sqrt{\beta}$), and those for δ_z are imaginary numbers [$s=\pm\sqrt{P(X_0,\mu)}i$]. Therefore, the motions of $\boldsymbol{\delta}$ are obtained as follows:

$$\begin{cases}\delta_x = C_1e^{\sqrt{\alpha}t}+C_2e^{-\sqrt{\alpha}t}+C_3e^{\sqrt{\beta}t}+C_4e^{-\sqrt{\beta}t}\\ \delta_y = C_5e^{\sqrt{\alpha}t}+C_6e^{-\sqrt{\alpha}t}+C_7e^{\sqrt{\beta}}t+C_8e^{-\sqrt{\beta}t}\\ \delta_z = C_9\cos\sqrt{P(X_0,\mu)}t+C_{10}\sin\sqrt{P(X_0,\mu)}t\end{cases} \tag{54}$$

where $C_i(i=1,\ldots,10)$ are constants of integration. It is found that δ_x and δ_y contain only divergence or damping terms.

When we set $\omega_z(X_0,\mu)=\sqrt{P(X_0,\mu)}$ and choose only the oscillation term from these equations, the motions are rewritten as

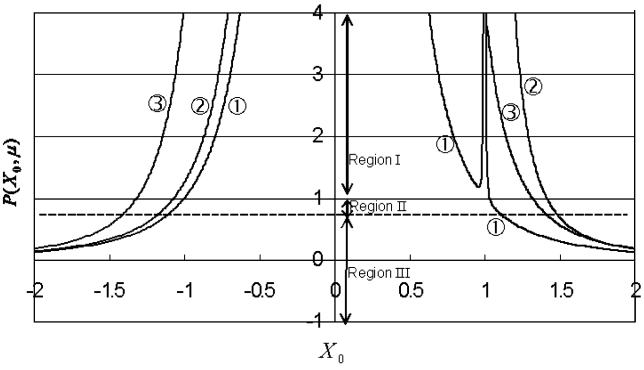

① μ = 3.04e-6 (Sun-Earth), ② μ = 0.1,and ③ μ = 0.5

Fig. 3 $P(X_0,\mu)$ with respect to X_0.

$$\begin{cases}\delta_x = 0\\ \delta_y = 0\\ \delta_z = C_z\cos(\omega_z t+\phi_z)\end{cases} \tag{55}$$

D. Parameter $P(X_0,\mu)$

In general there are two or more values of X_0 for a given value of $P(X_0,\mu)$ at one mass ratio. For example, when the mass ratio corresponds to the sun–Earth system and $P(X_0,\mu)=1$ (see Fig. 3), there is one value of X_0 in $X_0>0$ and one value of X_0 in $X_0<0$. On the other hand, when the mass ratio corresponds to the sun–Earth system and $P(X_0,\mu)=2$, there is one value of X_0 in $X_0>0$ and three values of X_0 in the $X_0<0$ region.

Figures 4 and 5 show the acceleration with respect to $P(X_0,\mu)$ in the stable region (region II). The value of acceleration in Fig. 4 is dimensionless whereas that in Fig. 5 is depicted with units, which is derived from the mass ratio μ and the distance between the primary bodies. From Fig. 4, we find that the dimensionless magnitude of acceleration gets smaller as $P(X_0,\mu)$ and the mass ratio μ gets larger. In Fig. 5, the required acceleration for the sun–Jupiter system is the smallest because the distance between Jupiter and the sun is much larger than in the Earth–sun and Mars–sun systems.

IV. Resonant Periodic Orbits

In this section, the frequencies of the solutions δ_x, δ_y, and δ_z are considered. When the frequencies of δ_x and δ_y (i.e., ω_α, ω_β) and that of δ_z (i.e., ω_z) differ slightly, projections of the orbits become Lissajous curves. If the frequencies of δ_x and δ_y and that of δ_z are the

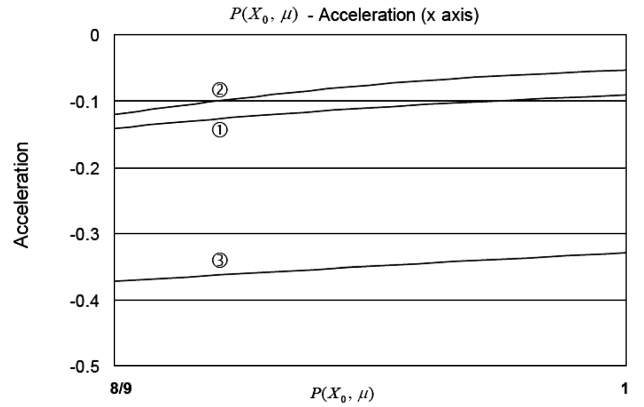

① m = 3.04e-6 (Sun-Earth), ② m = 3.23e-7 (Sun-Mars), ③ m = 9.54e-4 (Sun-Jupiter)

Fig. 4 Normalized acceleration with respect to $P(X_0,\mu)$ in the stable region (region II).

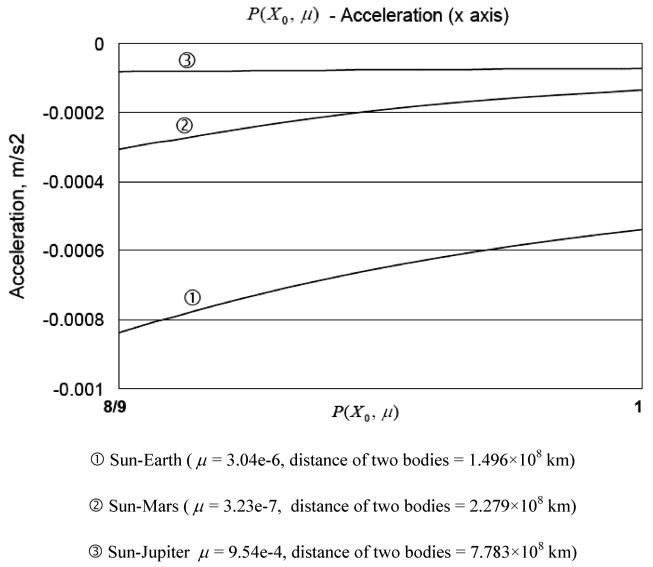

Fig. 5 Specific acceleration with respect to $P(X_0, \mu)$ in the stable region (region II).

same or are a simple integer ratio, such as 1:1 or 1:2, then a spacecraft achieves a periodic orbit. Table 1 shows values of $P(X_0, \mu)$, at which ω_α or ω_β and ω_z have simple integer ratios. When ω_α and ω_β are larger than ω_z, there is no value of $P(X_0, \mu)$ satisfying the simple integer ratio. As for ω_β, the integer ratio of ω_β:$\omega_z = 1$:1 is the only solution. From Eqs. (40) and (41), ω_α is smaller than ω_β at the same point, so that a spacecraft with a frequency ω_β orbits more slowly than one with a frequency of ω_α.

Now numerical examples of resonant periodic orbits using the nonlinear equations of motion, Eq. (4), are shown (see Fig. 6). The acceleration is assumed to be constant as in Eq. (9). The mass ratio is assumed to be $\mu = 3.0404 \times 10^{-6}$, and the distance between two bodies is 1.496×10^{11} m which corresponds to the mass ratio of the sun–Earth system. The amplitudes of δ_x, δ_y, and δ_z, which indicate the size of the orbit, are set at 15 km. The initial points are obtained from Eqs. (48) and (51), or (52), and the initial velocities are obtained by differentiating the initial positions. Substituting these initial conditions and accelerations into Eq. (4) and integrating numerically, the periodic orbits are obtained. Figure 6 shows the comparison between the analytical solutions and the numerical one. Because the size of the periodic orbits is small (15 km), the error between the nonlinearized Eq. (4) and linearized Eq. (12) can be neglected.

Figure 7 shows the resonant periodic orbits shown in Table 1 when $X_0 > 0$. Similar figures can be found when $X_0 < 0$. The artificial equilibrium point, acceleration vector, and periods of orbit are also shown in Fig. 7. Note that the scale of δ_x–δ_z projections for the cases of ω_β:$\omega_z = 1$:3 and 1:4 differ from the other projections.

V. Discussion

Artificial equilibrium points are proposed using constant low-thrust acceleration. Furthermore, periodic orbits around these artificial equilibrium points are generated analytically in which the initial conditions are obtained from the linearized equations of motion. The proposed method can generate small-size artificial

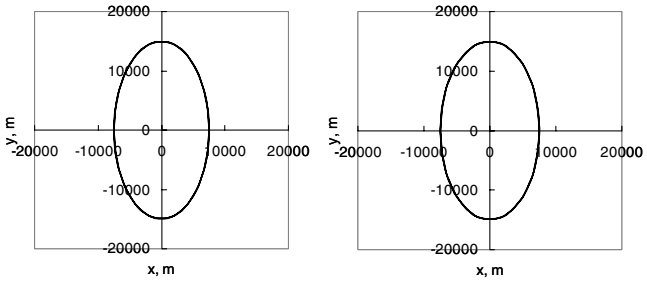

Fig. 6 Comparison between the analytical solution and the numerical solution (orbit size is 15 km): a) analytical solution; b) numerical solution.

halo-type orbits in an efficient way. These periodic orbits are in three-dimensional space, which realize local periodic motion around artificial equilibrium points and are applicable, for example, to asteroid hovering missions and space weather missions in the sun–Earth system requiring local periodic motion for observation. The possibility of large-size halo-type orbits is discussed later in this section.

By choosing the frequencies of motions that are small-integer resonant, we found the existence of points at which in-plane and out-of-plane motions are synchronized. When $P = 1$, the period of in-plane motion equals that of the out-of-plane motion. Moreover, the periods are $\omega_\beta = \omega_z = 1$, which means that these solutions are periodic in both the rotating and the inertial frames.

For periodic orbits in the stable region (see Fig. 2), the control acceleration required takes the values shown in Figs. 4 and 5. When the control acceleration around an artificial equilibrium point is changed, then the center point of periodic orbits may be shifted to another artificial equilibrium point as a function of the control acceleration. This means we can switch from a periodic orbit to another periodic orbit by changing the control acceleration appropriately.

The limitation arising from a linearized approach is shown in Figs. 8–11. Each center of the two periodic orbits in Figs. 8–11 is assumed to exist at $X = 1.02$ (region I in Fig. 2) and at $X = 1.03223$ (ω_β:$\omega_z = 1$:1 in region II in Fig. 2), respectively. The integration time in this simulation is 3 years. For linear and nonlinear orbits of the same size in Figs. 8–11, the amplitudes A, A_z of Eq. (48) and B, B_z of Eq. (52) are 1.0×10^{-5} AU (about 1.5×10^6 m) and 1.0×10^{-4} AU (about 1.5×10^7 m), respectively. As for the larger nonlinear orbits in Figs. 8–11, the amplitudes A, A_z and B, B_z are 1.0×10^{-4} AU (about 1.5×10^7 m) and 1.0×10^{-3} AU (about 1.5×10^8 m), respectively. The initial phases of Eqs. (48) and (52) are set to $\phi_{xy} = 0$, $\phi_z = 0$. The shapes of the smaller nonlinear orbits are the same as those of the linear orbits. From these figures, the limitation of size is found to be from 1.5×10^6 m to 1.5×10^8 m, when the spacecraft cannot complete more than one revolution in its periodic orbit. However these linearized orbits are useful to develop large-amplitude orbits in the nonlinear system. Figure 12 shows an example of orbits using nonlinear equations of motion [Eq. (8)]. The initial positions are the same as those of Figs. 10c and 11c, whereas the velocity in the y component is varied to achieve large-amplitude periodic motion. The velocity in the y component of the linear case is 0 m/s, and that of the nonlinear case is −0.12 m/s.

Table 1 Values of $P(X_0, \mu)$ that satisfy ω_α or ω_β and form a simple integer ratio with ω_z. The — notation stands for "no solution"

	ω_α:ω_z or ω_β:ω_z						
	1:1	1:2	2:1	1:3	3:1	1:4	4:1
ω_α	—	$P(X_0, \mu) = 0.93 \begin{pmatrix} \omega_\beta = 0.48 \\ \omega_z = 0.97 \end{pmatrix}$	——	$P(X_0, \mu) = 0.97 \begin{pmatrix} \omega_\beta = 0.33 \\ \omega_z = 0.98 \end{pmatrix}$	——	$P(X_0, \mu) = 0.98 \begin{pmatrix} \omega_\beta = 0.25 \\ \omega_z = 0.99 \end{pmatrix}$	——
ω_β	$P(X_0, \mu) = 1.00 \begin{pmatrix} \omega_\beta = 1.00 \\ \omega_z = 1.00 \end{pmatrix}$	——	——	——	——	——	——

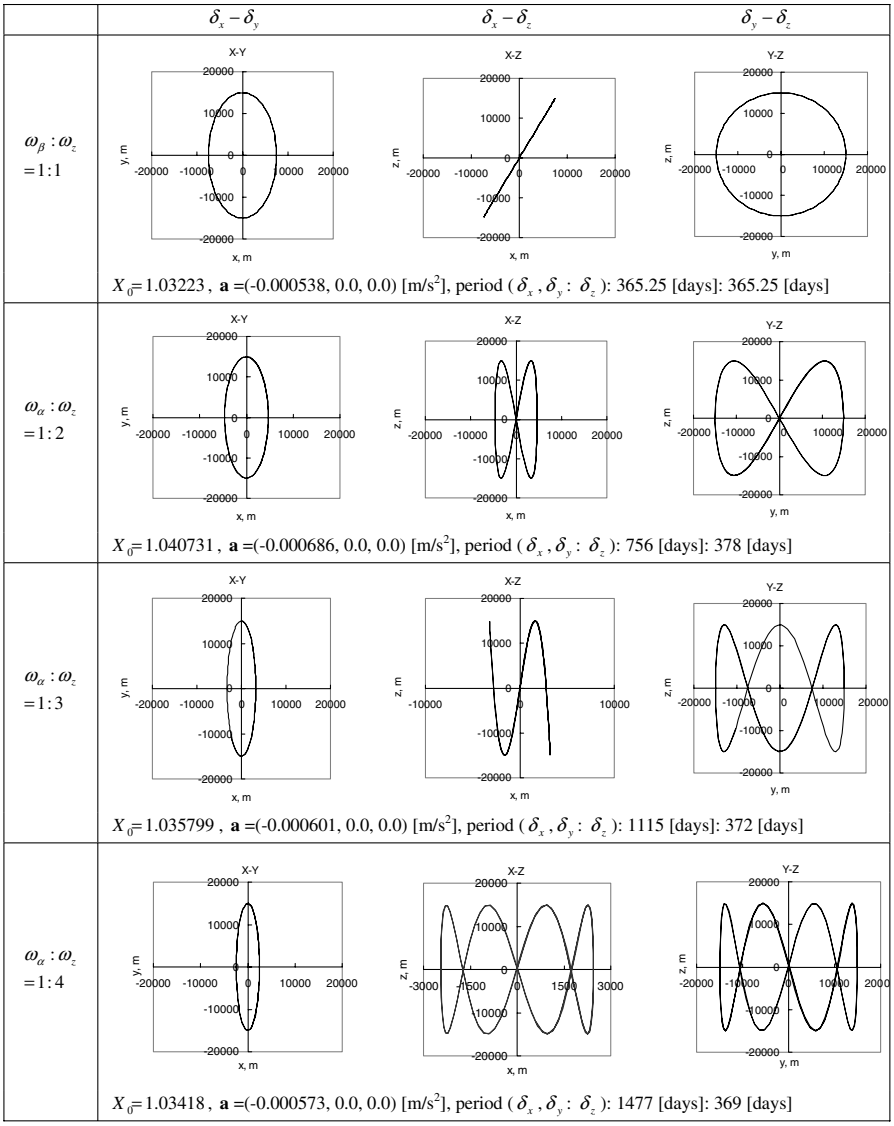

Fig. 7 Synchronous periodic orbits.

The direction and magnitude of control acceleration in this paper is kept constant during a periodic orbit. In general, the acceleration direction of the solar sail depends on its sail steering capability and cannot be turned to the sun. The magnitude of thrust of a solar sail is dependent on the steering angle and the sail area. On the other hand, the magnitude of solar electric propulsions (SEP) is dependent on the available electrical power. Therefore to obtain a constant acceleration we must control the power budget. Because SEP consumes the propellant and causes the mass of the spacecraft to decrease, the thrust must be controlled as the propellant is consumed in order to achieve a constant acceleration.

In the example in Fig. 7, the directions of accelerations for all cases are sunward. It is therefore difficult for solar sails to generate these orbits. The magnitudes of the accelerations are dependent on the mass ratio μ and the distance between the two primary bodies as shown in Figs. 4 and 5. For example, the required acceleration magnitude of the $\omega_\beta{:}\omega_z = 1{:}1$ case in the sun–Earth system is 0.000538 m/s^2 and this corresponds to about 500 mN thrust for 1000 kg spacecraft and 250 mN thrust for 500 kg spacecraft. On the other hand, the required acceleration in the sun–Jupiter system is about 0.0001 m/s^2 and this corresponds to about 100 mN thrust for 1000 kg and 50 mN thrust for 500 kg. These values can be achieved by existing SEP systems such as the NSTAR engine (about 90 mN) [13] used on the DS1 spacecraft. Assuming a specific impulse (Isp) of 3200 s and a propellant mass percentage of 50%, the time until the propellant is depleted is 337 days in the sun–Earth system and 1815 days in the sun–Jupiter system, respectively. When periodic orbits exist on the point $X_0 = -1.000002$ which satisfy the $\omega_\beta{:}\omega_z = 1{:}1$ condition ($P = 1$) in $X_0 < 0$, the required acceleration magnitude is drastically reduced to 1.3×10^{-9} m/s^2. If nonresonant periodic orbits are considered, the acceleration requirement can be reduced further still. For example, the required acceleration magnitude of periodic orbits at $X_0 = 1.009$ in the sun–Earth system is 0.0000637 m/s^2, which corresponds to ~60 mN thrust for a 1000 kg spacecraft. In this case, the direction of acceleration is opposite to the sun, and therefore a solar sail system can be used.

VI. Conclusion

Periodic orbits around nonequilibrium points were generated analytically by changing these points into artificial equilibrium points with low-thrust acceleration. The equations of motion were linearized about a nonequilibrium point, which corresponds to the center of oscillatory motion. The characteristic equations for the equations of motion were transformed into a cubic function. Oscillatory motions were obtained by determining the initial conditions such that the divergence term is canceled. As a special case, periodic orbits centered on the line connecting the primary bodies were investigated. The orbits were divided into various types based on a parameter that expresses the relationship between the

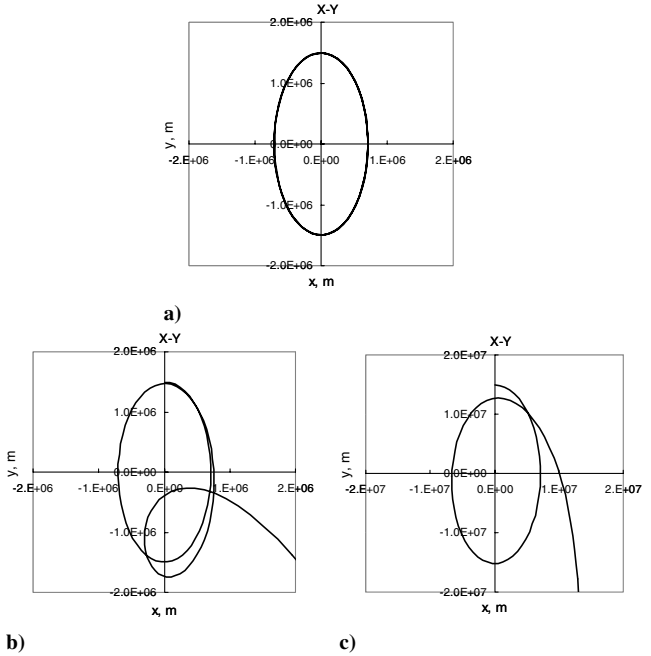

Fig. 8 The in-plane limitation of linearization [$X_0 = 1.02$ (region I in Fig. 2)]: a) linear orbit (size: 1.0×10^6 m), b) nonlinear orbit (size: 1.0×10^6 m), c) nonlinear orbit (size: 1.0×10^7 m).

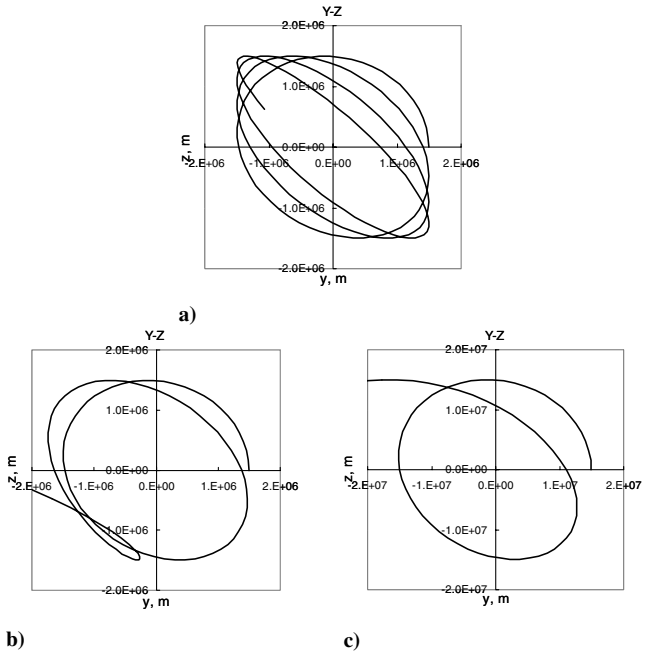

Fig. 9 The out-of-plane limitation of linearization [$X_0 = 1.02$ (region I in Fig. 2)]: a) linear orbit (size: 1.0×10^6), b) nonlinear orbit (size: 1.0×10^6 m), c) nonlinear orbit (size: 1.0×10^7 m).

mass ratio and the position of an artificial equilibrium point. It was shown that by choosing an appropriate center point and acceleration, the frequencies of in-plane and out-of-plane motion have simple integer ratios, and resonant periodic orbits can be realized. Periodic orbits with constant acceleration can be generated in the nonlinear equations of motion by choosing the appropriate initial conditions obtained from the linear equations. The proposed periodic orbits around artificial equilibrium points are applicable to hovering missions which require station keeping at nonequilibrium points. Because the periodic orbits are in three-dimensional space, these orbits may be especially useful for regular-interval observations from out-of-plane positions.

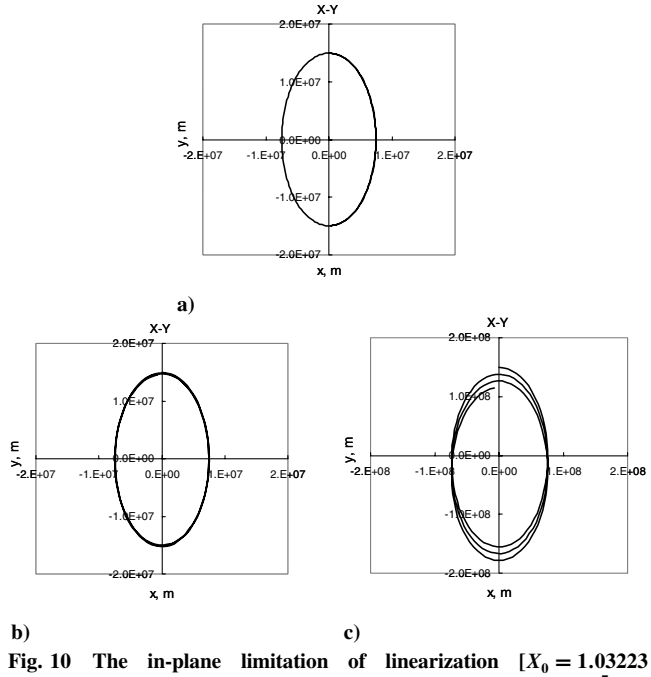

Fig. 10 The in-plane limitation of linearization [$X_0 = 1.03223$ (ω_β:$\omega_z = 1$:1 in region II)]: a) linear orbit (size: 1.0×10^7 m), b) nonlinear orbit (size: 1.0×10^7 m), c) nonlinear orbit (size: 1.0×10^8 m).

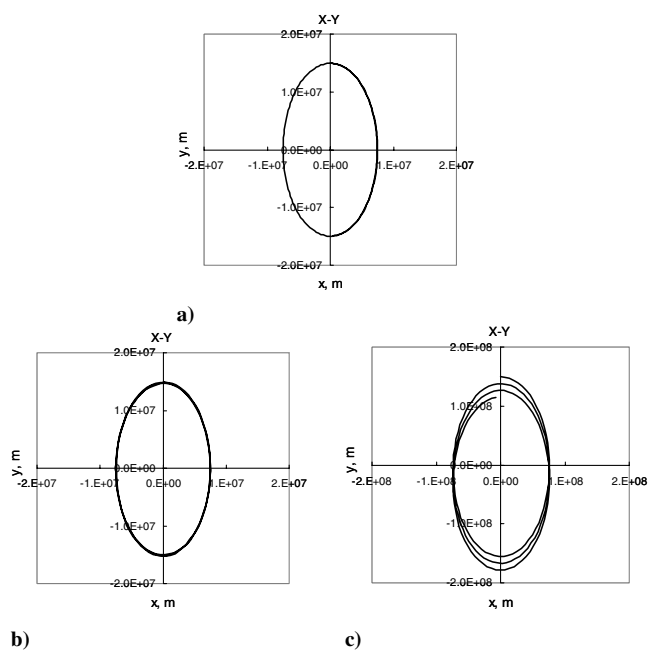

Fig. 11 The out-of-plane limitation of linearization [$X_0 = 1.03223$ (ω_β:$\omega_z = 1$:1 in region II)]: a) linear orbit (size: 1.0×10^7 m), b) nonlinear orbit (size: 1.0×10^7 m), c) nonlinear orbit (size: 1.0×10^8).

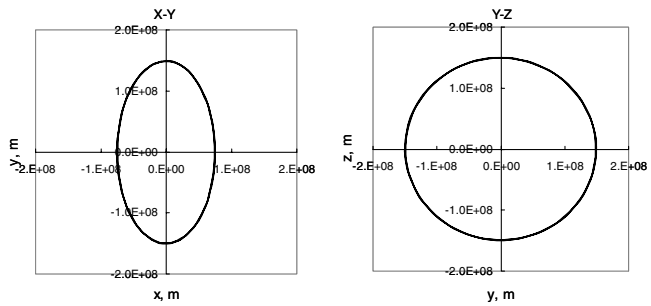

Fig. 12 Large-amplitude nonlinear orbits (size: 1.0×10^8 m) in the x–y plane and the y–z plane [$X_0 = 1.03223$ (ω_β:$\omega_z = 1$:1 in region II)].

Acknowledgments

The authors would like to express their appreciation to D. J. Scheeres of the University of Michigan and H. Yano of the Japan Aerospace Exploration Agency for their valuable discussions and constructive suggestions that have improved this manuscript greatly. We are also thankful to the anonymous referees and the associate editor for their in-depth comments.

References

[1] Broucke, R., "Stability of Periodic Orbits in the Elliptic, Restricted Three-body Problem," *AIAA Journal*, Vol. 7, No. 6, 1969, pp. 1003–1009.

[2] Farquhar, R. W., "The Control and Use of Libration-Point," NASA TR R-346, 1970.

[3] Farquhar. R. W., and Kamel, A. A., "Quasi-Periodic Orbits About the Translunar Libration Point," *Celestial Mechanics*, Vol. 7, No. 4, 1973, pp. 458–473.

[4] Jorba, A., and Masdemont, J., "Dynamics in the Center Manifold of the Collinear Points of the Restricted Three Body Problem," *Physica D*, Vol. 132, No. 1-2, 1999, pp. 189–213.

[5] Gómez, G., and Mondelo, J. M., "The Dynamics Around the Collinear Equilibrium Points of the RTBP," *Physica D*, Vol. 157, No. 4, 2001, pp. 283–321.

[6] Dusek, H. M., "Motion in the Vicinity of Libration Points of a Generalized Restricted Three-Body Model," *Methods in Astrodynamics and Celestial Mechanics*, edited by R. L. Duncombe and V. G. Szebehely, Vol. 17, Progress in Astronautics and Aeronautics, AIAA, New York, 1966, pp. 37–54.

[7] Simmons, J. F. L., McDonald, A. J. C., and Brown, J. C., "The Restricted 3-Body Problem with Radiation Pressure," *Celestial Mechanics*, Vol. 35, No. 2, 1985, pp. 145–187.

[8] McInnes, C. R., McDonald, A. J., Simmons, J. F. L., and MacDonald, E., "Solar Sail Parking in Restricted Three-Body Systems," *Journal of Guidance, Control, and Dynamics*, Vol. 17, No. 2, 1994, pp. 399–406.

[9] Scheeres, D. J., Hsiao, F. Y., and Vinh, N. X., "Stabilizing Motion Relative to an Unstable Orbit: Applications to Spacecraft Formation Flight," *Journal of Guidance, Control, and Dynamics*, Vol. 26, No. 1, 2003, pp. 62–73.

[10] Broschart, S. B., and Scheeres, D. J., "Control of Hovering Spacecraft Near Small Bodies: Application to Asteroid 25143 Itokawa," *Journal of Guidance, Control, and Dynamics*, Vol. 28, No. 2, 2005, pp. 343–354.

[11] Szebehely, V., *Theory of Orbits: the Restricted Problem of Three Bodies*, Academic Press, New York, 1967.

[12] Murray, C. D., and Dermotte, S. F., *Solar System Dynamics*, Cambridge Univ. Press, Cambridge, England, U.K., 2001, Chap. 3.

[13] Rayman, M. D., Varghese, P., Lehman, D. H., and Livesay, L. L., "Results from the Deep Space 1 Technology Validation Mission," *Acta Astronautica*, Vol. 47, No. 2, 2000, pp. 475–487.